



Enhanced analog-optical link performance with noiseless phase-sensitive fiber optical parametric amplifiers

Downloaded from: <https://research.chalmers.se>, 2021-08-31 10:52 UTC

Citation for the original published paper (version of record):

Zhao, P., Kakarla, R., Karlsson, M. et al (2020)

Enhanced analog-optical link performance with noiseless phase-sensitive fiber optical parametric amplifiers

Optics Express, 28(16): 23534-23544

<http://dx.doi.org/10.1364/OE.397999>

N.B. When citing this work, cite the original published paper.



Enhanced analog-optical link performance with noiseless phase-sensitive fiber optical parametric amplifiers

PING ZHAO,^{*}  RAVIKIRAN KAKARLA, MAGNUS KARLSSON, AND PETER A. ANDREKSON 

Photonics Laboratory, Department of Microtechnology and Nanoscience, Chalmers University of Technology, SE-412 96 Gothenburg, Sweden

^{*}pingz@chalmers.se

Abstract: In this paper, we investigate the enhancement of analog optical link performance with noiseless phase-sensitive fiber optical parametric amplifiers. The influence of different noise sources in the link impacts the quality of analog optical signals, especially with low optical signal power, which has not been investigated before. Theoretically, the increase in signal-to-noise ratio and spurious-free dynamic range can be up to ~6 dB and ~4 dB, respectively, if the noise figure of optical pre-amplifier drops 3 dB when the received optical power is less than -65 dBm. In addition, experiments based on a 1.3 dB-noise-figure phase-sensitive fiber optical parametric amplifier and conventional optical pre-amplifiers are implemented, and the measured results agree with the theoretical expectations. This illustrates that noiseless phase-sensitive optical amplification may pave the way to long-haul distribution of analog optical signals and find applications in microwave-photonic systems.

© 2020 Optical Society of America under the terms of the [OSA Open Access Publishing Agreement](#)

1. Introduction

With the advantages of large bandwidth, long reach, immunity to electro-magnetic interference and high operational flexibility, microwave photonic technologies have been widely investigated in the past two decades [1,2] and continues to attract interest in recent years [3,4]. Processing of analog optical signals is of great importance in microwave-photonic systems [5], including electro-optical/opto-electrical conversion [6] and advanced filtering [7,8]. With the development of ranging techniques, multiple-input-multiple-output (MIMO) radar with widely separated antennas is attracting vast research interest [9–12]. These antennas are distributed at different areas with distances varying from several to hundreds of kilometers and connected to one central station via analog optical links (AOLs). In this scenario, analog optical signals from some antennas far away from the central station may suffer from huge link losses. Improving the signal-to-noise ratio (SNR) and the third-order spurious-free dynamic range (SFDR3) of individual AOLs is beneficial to increase the number of antennas in MIMO radar systems and helps to enhance the sensitivity and the detection area. Conventional techniques have been widely investigated to improve the performance of AOLs, including optimizing analog optical transmitters [13–16] and receiver [17]. Optical pre-amplifiers (OPAs) are effective components to enlarge the reach/margin of long-haul AOLs [18,19] and fully compatible with those conventional techniques. Due to its natural wideband property, an OPA can support the transmission of multi-channel analog optical signals which is promising in microwave photonics as well. Compared with conventional Erbium-doped fiber amplifiers (EDFAs) having an intrinsic 3-dB noise figure (NF) limit [20], noiseless OPAs may be beneficial since they can improve the signal-to-noise ratio (SNR) of the output signal. Phase-sensitive parametric optical amplifiers based on second- or third-order nonlinear optical effects can enable noiseless amplification in principle [21], and have exhibited promising low-noise properties [22,23]. Owing to low NF and high gain, phase-sensitive fiber

parametric optical amplifiers (PS-FOPAs) have been intensively investigated, and shown to greatly enlarge the transmission distance of digital optical signals over fiber [24,25], thereby facilitating highly sensitive and high-capacity free-space optical communication [26]. Besides, the PS-FOPA is also attracting increasing interest in analog optical signal processing [27–29]. Low-noise amplification of analog optical signal was experimentally investigated by Lim et al. in 2008 [27]. Then Agarwal et al. preliminarily demonstrated that PS-FOPA could improve the SFDR3 of the AOL [28]. Tarek et al. showed that PS-FOPA did not induce nonlinearity to the analog RF signal of the AOL via simplified experiments [29]. However, the improvements in the AOL performance in these demonstrations were limited by the implementation penalties of unoptimized PS-FOPAs since the pump frequency was phase modulated to suppress the stimulated Brillouin scattering (SBS) in highly-nonlinear fibers (HNLFs). Moreover, the power of the received optical signal will be weak due to the potentially huge link loss in AOLs. The large variation of the input optical signal power into the PS-FOPA may have distinct influences on the AOL performance, which has not been investigated yet.

In this paper, we investigate AOLs with different OPAs and find that the system performance can be enhanced due to the low-noise property of PS-FOPA which uses strained HNLFs without phase modulating the pump. Based on theoretical modeling of a two-tone AOL [5], it is found that the SNR of the AOL output RF signal can be efficiently improved due to the decrease in the NF of the OPA. As practical optical bandwidths are usually larger than the RF frequency band of conventional AOLs, the improvement in the SNR of the output analog RF signal is obvious when the input optical signal power of the OPA is low, i.e., less than -55 dBm, since the noise-noise beating from the optical amplified spontaneous emission (ASE) becomes dominant. Moreover, the SFDR3 of the AOL increases with the SNR. In addition to the theoretical work, we have built experimental AOL setups and compared a PS-FOPA (NF = ~1.3 dB), a phase-insensitive fiber optical parametric amplifier (PI-FOPA, NF = ~3.9 dB) and an EDFA (NF = ~4.3 dB) as OPAs, respectively. The SNR increases about 3 dB for -40-dBm input optical signal when the EDFA is replaced by the PS-FOPA. This increase further reaches 5.5 dB when the optical signal power fed to the analog optical receiver is -70 dBm. Additionally, an improvement of about 4 dB in the SFDR3 of the AOL is obtained. These experimental results agree with the theoretical analysis and show that PS-FOPA has a bright potential in analog optical transmission and may contribute to unrepeated microwave photonic systems and networks.

2. Principle

2.1. Modeling of AOL with OPA

Two-tone testing is a common approach of characterizing the dynamic range of AOLs [5]. Figure 1 shows a typical model diagram of an AOL. Two equal-power RF tones are combined as the electrical signal source. At the transmitter (Tx), a Mach-Zehnder modulator (MZM) is utilized for electrical-to-optical conversion, as the second-harmonic term can be mitigated when a proper bias voltage (V_B) is applied [5]. Transmission of the analog optical signal modulated by RF frequencies is emulated by an element loss. Here, we focus on the reception of low-power analog optical signals in which case optical amplification is needed. An OPA at the receiver (Rx) side of the AOL improves the intensity of the analog optical signal. An optical band-pass filter (OBPF) reduces the optical noise mixed with the amplified optical signal. Then, a photodetector (PD) performs the optical-to-electrical conversion and outputs an RF signal. The PD-input optical power, P_{PD} , is set to be constant and kept to maintain the linear range of the PD. The power of the output RF signal can be written as [30]

$$P_S = \frac{1}{32} \left(\frac{\pi V_m}{V_\pi} \right)^2 \left[r_{PD} G_O P_{OA, in} \sin \left(\frac{\pi V_B}{V_\pi} \right) \right]^2 R_L \quad (1)$$

where V_m is the amplitude of the input RF tone, V_π is the half-wave voltage of the MZM, r_{PD} is the PD responsivity, G_O is the gain of the OPA, $P_{OA,in}$ is the optical power received by the Rx and R_L is the load resistance. Additionally, there is thermal, relative-intensity, shot and ASE-related noise generated. The noise induced by optical amplification is dominant in the AOL and mainly consists of two parts, optical signal-ASE beat noise $\sigma_{s-sp}^2 = 2q\eta r_{PD} G_O^2 N F_O P_{OA,in} B_e$, and ASE-ASE beat noise $\sigma_{sp-sp}^2 = 2(q\eta G_O N F_O)^2 B_O B_e$, where σ^2 is the variance of the noise current, q is the electron charge, η is the quantum efficiency of the PD, $N F_O$ is the NF of the OPA, B_O and B_e are the bandwidths of the OBPF and electrical band-pass filter of the AOL, respectively [20]. The thermal, relative-intensity, and shot noise can be neglected when the input optical signal power of the OPA is small. As a result, the output noise power of the AOL can be regarded as $P_N \approx (\sigma_{s-sp}^2 + \sigma_{sp-sp}^2) R_L / 4$ [22]. We assume that the MZM is biased at $V_\pi/2$. The SNR of the output RF signal can be approximated by

$$SNR \approx \frac{1}{16} \left(\frac{\pi V_m}{V_\pi} \right)^2 \frac{(r_{PD} P_{OA,in})^2}{q\eta r_{PD} N F_O P_{OA,in} B_e + (q\eta N F_O)^2 B_O B_e}. \quad (2)$$

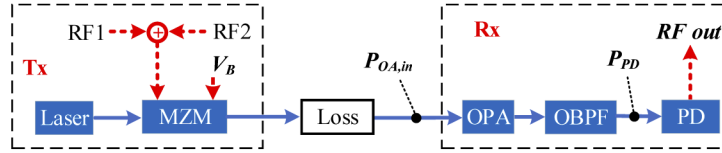


Fig. 1. Model of an AOL for two-tone test.

Additionally, due to the nonlinearity of the MZM, second- and third-order intermodulation distortions (IMD2, IMD3) arise. Being far away from the source frequencies, IMD2 is not addressed in this paper since they can be greatly suppressed by controlling the MZM bias voltage [30] and blocked by further electrical filters. As the IMD3 is quite close to the target frequency regime, it can hardly be well mitigated by a static filter and its power can be expressed as [30]

$$P_{IMD3} = \frac{1}{64} \left(\frac{\pi V_m}{V_\pi} \right)^4 P_S. \quad (3)$$

Letting the power of IMD3 equal the noise power, the SFDR3 of the AOL can be obtained as

$$SFDR3 \approx \left[\frac{(r_{PD} P_{OA,in})^2}{2q\eta r_{PD} N F_O P_{OA,in} B_e + 2(q\eta N F_O)^2 B_O B_e} \right]^{2/3}. \quad (4)$$

According to Eqs. (2) and (4), both the signal-ASE and ASE-ASE beat noises will influence the SNR and SFDR3 of the AOL. Here, we define a ratio of signal-ASE to ASE-ASE beat noise, $\alpha = \sigma_{s-sp}^2 / \sigma_{sp-sp}^2$, which is expressed as

$$\alpha = \frac{P_{OA,in}}{h\nu_0 N F_O B_O} \quad (5)$$

where h is the Plank constant and ν_0 is optical frequency. It is clear that α depends on the optical bandwidth of the AOL, the input optical signal power of the Rx and the NF of the OPA. Consider a constant optical power into the PD. For a relatively-high $P_{OA,in}$, the signal-ASE beating dominates the total output noise. In this case, a 3-dB reduction in $N F_O$ can roughly increase the SNR of the output RF signal by 3 dB and improve the AOL's SFDR3 by ~2 dB. On the other hand, the ASE-ASE beat noise may surpass the signal-ASE beat noise when the Rx-input optical signal

power drops to a low level for a specific OBPF bandwidth and NF, according to Eq. (5). As a result, a 3-dB improvement in NF_O may lead to ~6 dB and ~4 dB increases in the output SNR and SFDR3 of the AOL, respectively. Generally, the RF frequency of the AOL is narrower than the OBPF bandwidth (usually larger than 10 GHz in robust applications). This implies that low-NF OPAs will be preferred for AOLs suffering from large link losses.

2.2. Analysis

Figure 2 depicts the calculated optical bandwidth of the AOL as a function of the NF of the OPA for $\alpha = 1$ at two different RF frequencies and at two optical signal powers received by the Rx. In the calculation, r_{PD} is 1 A/W and η is 0.8. The blue and red solid lines correspond to the Rx-input optical signal power of -50 dBm and -55 dBm, respectively. The black dotted lines indicate the minimum link optical bandwidths which shall be at least twice of the RF frequency [4]. As can be seen, the optical bandwidth for equal the signal-ASE and ASE-ASE noises decreases with increasing the NF of the OPA. Figure 2(a) shows the case of an AOL with 1 GHz RF frequency. Regarding a typical NF (i.e., conventional EDFA) of 5.5 dB, the optical bandwidth is about 22 GHz if $P_{OA,in}$ equals -50 dBm, and it drops to 7 GHz for $P_{OA,in} = -55$ dBm. For a fixed optical bandwidth of 10 GHz, the NF of the OPA is 9.9 dB for $P_{OA,in} = -50$ dBm and 3.9 dB for $P_{OA,in} = -55$ dBm. Moreover, the case of a 5-GHz AOL is shown by Fig. 2(b). Due to the increase in the RF frequency, the optical bandwidth of the AOL needs to be larger than 10 GHz. As can be seen, the ASE-ASE beat noise will always be dominant when the NF is higher than 4 dB for $P_{OA,in} = -55$ dBm. In other words, a lower NF will help to mitigate the optical noise for the detection of low-power analog optical signals, particularly for high-RF-frequency AOLs.

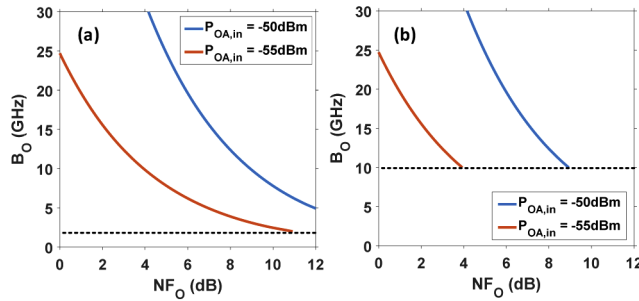


Fig. 2. Optical bandwidth varying with the NF of the OPA for $\alpha = 1$ at a central RF frequency of (a) 1 GHz and (b) 5 GHz. The blue and red solid lines correspond to the input optical signal power of -50 dBm and -55 dBm, respectively. The black dotted lines represent the lower boundaries of the optical bandwidths of the AOL.

We now theoretically investigate how these noises influence the SNR as well as SFDR3 of the AOL. Two RF tones with frequencies of 998 MHz and 1002 MHz are utilized. In the calculation, $V_{\pi} = 2.4$ V, $V_B = 1.2$ V, $r_{PD} = 1$ A/W and $\eta = 0.8$. The electrical bandwidth is 1 Hz and the OBPF has a bandwidth of 10 GHz (0.08 nm). Figures 3(a)-(c) presents the calculated output powers of the RF signal, IMD3 and noise of the AOL under three cases (Case I-III), respectively. The blue and orange lines correspond to the OPA's NF of 1 and 6 dB, respectively. Table 1 summarizes some typical parameters in the three cases. As can be seen in Fig. 3(a), the optical gain is different when the noise figure of optical amplifier changes for weak optical signals. The OSNR of the final output signal of the whole optical amplification module (cascaded optical amplifiers) can be expressed as $P_{OA,in}/(h\nu_0 B_S NF_O)$, where B_S is 12.5 GHz [20]. NF_O is the over-all noise figure of this optical amplification module and is almost equal to that of the first optical amplifier in the

module. The gain of the optical amplifier can be calculated according to

$$G_O = \frac{P_{OS}}{P_{OA,in}} = \frac{OSNR}{1 + OSNR} \frac{P_{PD}}{P_{OA,in}} = \frac{P_{PD}}{P_{OA,in} + h\nu_0 B_S N F_O} \quad (6)$$

where P_{OS} is the power of the final output optical signal. Since we fixed $P_{OA,in}$ and P_{PD} , the optical gain of the optical amplifier will change with the noise figure. In the two cases of Figs. 3(a) and (b), $P_{OA,in}$ is small, $G_O \approx P_{PD}/(h\nu_0 B_S N F_O)$. Hence, a 5-dB NF improvement leads to a 5-dB increase in optical current and a further ~ 10 dB increase in the power of the output RF signal for a given optical power into the PD. In this case, ASE-ASE beat noise dominates,

$$\sigma_{sp-sp}^2 \approx 2 \left(\frac{r_{PD} P_{PD}}{B_S} \right)^2 B_O B_e. \quad (7)$$

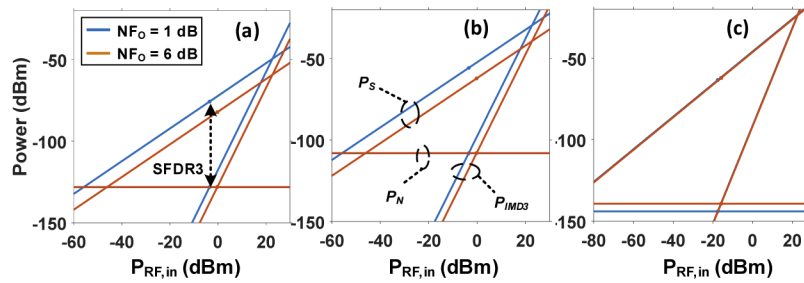


Fig. 3. Calculated SFDR3 curves of the AOL with an optical bandwidth of 10 GHz. The blue and orange lines correspond to the OPA's NF of 1 and 6 dB, respectively. The power of the optical signal into the Rx and the PD is (a) -70 dBm and -5 dBm, (b) -70 dBm and 5 dBm, and (c) -40 dBm and -5 dBm.

Table 1. Parameters of the AOLs.

Case	$P_{OA,in}$ (dBm)	P_{PD} (dBm)	NF_O (dB)	SNR(dB)@ $P_{RF,in} = 0$ dBm	SFDR3(dB/Hz ^{2/3})
I	-70	-5	1	55.8	52.3
			6	46	45.8
II	-70	5	1	55.8	52.3
			6	46	45.8
III	-40	-5	1	97.8	80.5
			6	93	77.2

Thus, the noise floor will not change with NF_O for a given P_{PD} when the optical signal power into the OPA is small. Additionally, we see from Fig. 3(a) a 6.5 dB/Hz^{2/3} improvement in SFDR3 can be obtained. When we use larger optical gain to increase the optical power received by the PD from -5 dBm to 5 dBm in Case II, the power of the output RF signal, IMD3 component and noise all increase accordingly, as shown in Fig. 3(b). The link SNR and SFDR3 do not change even as the optical power into the PD is increased, compared with Case I. This is because the power of the output RF signal, IMD3 component and noise all scale the same when P_{PD} changes if the ASE-ASE beat noise is dominant. For Case III illustrated by Fig. 3(c), the power of the RF signal does not change while the noise floor increases ~ 5 dB when the NF increases 5 dB. In this case, the signal-ASE beat noise, proportional to the product of Rx-input optical signal power and NF, is stronger than the ASE-ASE beat noise. Besides, the link SFDR3 is improved by 3.3 dB/Hz^{2/3} when NF_O drops from 6 dB to 1 dB. Hence, we can see an interesting process that the

improvement in the NF of the OPA enhances the RF signal intensity for low $P_{OA,in}$ and reduces the noise when $P_{OA,in}$ is high.

Moreover, we investigate how the NF of the OPA impacts the performance of the AOL with various $P_{OA,in}$. Figure 4(a) presents the calculated SNR (@ $P_{RF,in} = 0$ dBm, blue line) and SFDR3 (red line) as a function of the power of input optical signal of the OPA with an ideal 0 dB NF. The optical bandwidth of the AOL is set to be 2.1 GHz and the optical power in the PD is 5 dBm (a conventional output optical power level from a MZM in optical communications). The optical signal power into the analog Rx changes from -80 dBm to -5 dBm (i.e., a typical optical power below which optical amplification ($G_O > 10$ dB) is necessary) by adjusting the link loss. As can be seen, the SNR increases with $P_{OA,in}$ and the SFDR3 follows the same trend. The slope of the SNR- $P_{OA,in}$ curve begins to drop at around $P_{OA,in} = -60$ dBm. This is because that the ASE-ASE beat noise is dominant and nearly constant in the regime of $P_{OA,in} < -60$ dBm. According to Eqs. (2) and (4), 1 dB increase in $P_{OA,in}$ can result in ~ 2 dB and 1.33 dB/Hz^{2/3} improvements in SNR and SFDR3, respectively. With $P_{OA,in}$ increasing further, the signal-ASE beat noise gets stronger and the efficiency of improving the SNR and SFDR3 decreases. Here, we introduce two notations, $\Delta SNR = SNR(NF_O) - SNR(NF_O = 0 \text{ dB})$ and $\Delta SFDR3 = SFDR3(NF_O) - SFDR3(NF_O = 0 \text{ dB})$. The SNR and SFDR3 with $NF_O = 0$ dB are set to be baselines since they are the upper limits the AOL can reach without any optical noise. Figure 4(b) shows the calculated difference in the SNR of the AOL output signal varying with the Rx-input optical signal power for different NFs and link optical bandwidths. Two typical NFs, 3 dB (purple curves) and 6 dB (green curves), are chosen. The solid and dotted lines correspond to the cases of $B_O = 2.1$ GHz (slightly higher than twice of the RF frequency) and 15 GHz, respectively. Here, we define the improvement efficiency (τ) as the absolute value of ΔSNR (dB) divided by the NF change (dB). As can be seen from Fig. 4(b), τ is ~ 1 dB/dB when $P_{OA,in}$ changes from -10 dBm to -35 dBm where the signal-ASE beat noise is dominant for $B_O = 15$ GHz. It gradually saturates at ~ 2 dB/dB when $P_{OA,in}$ drops from -35 dBm to -80 dBm. In this $P_{OA,in}$ regime, ASE-ASE beat noise is constant, affected by the square of the NF of the OPA and gradually becomes the main part of the total noise during the drop of $P_{OA,in}$. This indicates that low NF will be preferred for the detection of weak analog optical signal. For higher signal power, i.e., $P_{OA,in} > -10$ dBm, τ decreases since the strength of shot and relative-intensity noise rises compared with the ASE-related noise when optical gain is small. Besides, the SNR difference (degradation) due to the NF_O increase can be slowed down by using narrow OBPFs. However, the bandwidth of practical robust optical filters is usually beyond 10 GHz and can hardly be less than 2 GHz [31]. From this point of

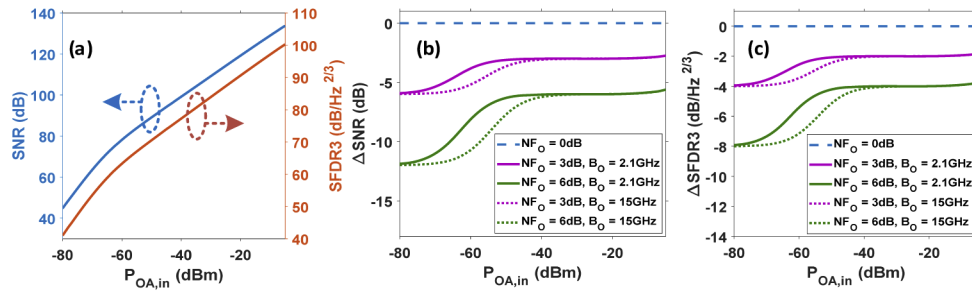


Fig. 4. (a) Calculated SNR (blue line) and SFDR3 (red line) varying with the power of the input optical signal of OPA for $B_O = 2.1$ GHz, $P_{PD} = 5$ dBm and $NF_O = 0$ dB. (b) ΔSNR and (c) $\Delta SFDR3$ of the AOL as a function of $P_{OA,in}$ with different NF_O and B_O . The case of $NF_O = 0$ dB is a baseline, denoted by the dashed blue curves. The purple and green curves correspond to $NF_O = 3$ dB and 6 dB, and the solid and dotted lines are for the cases of $B_O = 2.1$ GHz and 15 GHz, respectively.

view, low-NF OPAs can the requirement on OBPFs for the reception of weak analog optical signals. In addition, Fig. 4(c) shows the calculated difference in the SFDR3 of the AOL as a function of the Rx-input optical signal power. These SFDR3 curves evolves almost the same with those of the SNR. As can be seen, 3-dB change in the NF of the OPA can lead to a change of $2\text{-dB}/\text{Hz}^{2/3}$ in SFDR3 for $P_{OA,in} = -35\text{ dBm}$ for $B_O = 15\text{ GHz}$. This SFDR3 change can be enlarged to a saturated value of $4\text{ dB}/\text{Hz}^{2/3}$ when $P_{OA,in}$ is -80 dBm . The relative change between the intensity of signal-ASE and ASE-ASE beat noise accounts for the variation of ΔSFDR3 due to NF_O when $P_{OA,in}$ changes from -35 dBm to -80 dBm . Since the required optical bandwidth of the AOL will be expanded greatly if the RF frequency further increases, low-noise PS-FOPAs will be even more advantageous in processing wideband analog optical signals.

3. Experiments and results

3.1. Experimental setup

The experimental setup of a PS-FOPA-based AOL is depicted by Fig. 5(a). We use two conventional analog RF frequencies, i.e., 998 MHz and 1002 MHz, as the RF source to perform two-tone test. A tunable laser (CoBriteDX, IPD photonics) emits a single-polarization optical carrier (1550.64 nm), which is connected to a MZM (FTM7938EZ, Fujitsu, $V_\pi \sim 2.4\text{ V}@1\text{GHz}$) with a polarization-maintaining fiber patch cord. The two RF tones are combined by an electrical combiner and sent into the MZM to modulate the intensity of the optical carrier. The bias voltage of the MZM is optimized by minimizing the IMD2 term of the AOL output. Two equal sidelobes are generated simultaneously around the carrier wavelength on the optical spectrum. Due to the small frequency difference between the two RF tones, one sidelobe covers the two RF tones for illustration. To implement the PS-FOPA, we use a copier scheme at the Tx which has the advantage of being transparent to modulation formats [24]. The generated analog optical signal is combined with a narrow-linewidth continuous-wavelength (CW) pump (1554.32 nm, NKT Photonics, amplified by a high-power EDFA) using a wavelength-division multiplexer (WDM1). The power of the optical signal and pump is set to be 0 dBm and $\sim 30\text{ dBm}$, respectively. Then they are sent into a $\sim 50\text{ m}$ -long strained highly nonlinear optical fiber (HNLF, OFS) to generate an idler (conjugated copier of the optical signal) via four-wave mixing [32]. Then, the signal and idler are separated from the pump by WDM2 and transmitted to the Rx.

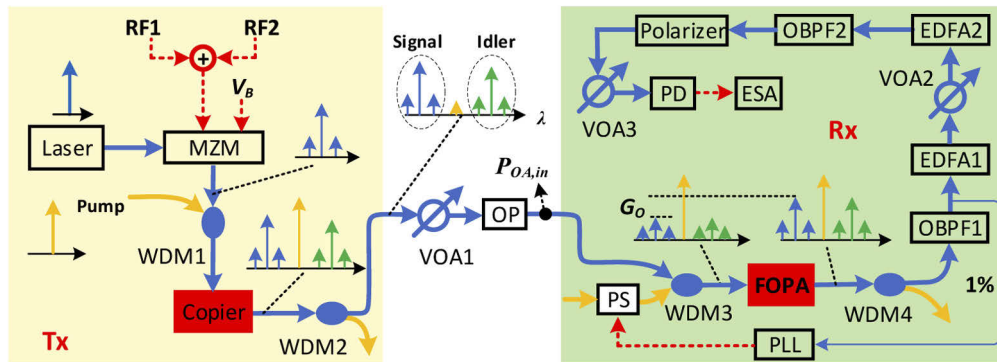


Fig. 5. Experimental setup of the AOL for the two-tone test. WDM, wavelength-division multiplexer. VOA, variable optical attenuator. OP, optical processor (programmable optical filter). PS, phase shifter. PLL, phase lock loop. ESA, electrical signal analyzer.

A variable optical attenuator (VOA) is used to emulate the optical fiber transmission. An optical processor (OP, Waveshaper, FINISAR) is utilized to balance the power of the signal and idler to maximize phase-sensitive gain. At the Rx, the signal and idler are combined with

the pump (~ 29 dBm) by WDM3 and fed to the FOPA which consists of four cascaded spools of strained HNLFs (HNLF-SPINE with λ_0 at ~ 1543 nm, OFS). These HNLFs with lengths of 101, 124, 156 and 205 m and having in-line isolators placed between are optimized to support the injection of high-power CW pump without frequency dithering [33]. For simplicity of implementation, the pump does not experience the emulated link loss and enters the Rx directly in our experiments. The FOPA output is connected to WDM4 to separate the amplified optical signal from the pump and idler. To reject the pump and idler, OBPF1 with a bandwidth of 2 nm is used. Then 1% of the OBPF1 output is extracted by a fiber coupler and used as the feedback of a phase lock loop (PLL) for adaptive control of the phase shifter (PS) to maximize the optical signal power. We characterize the properties of the PS-FOPA based on the optical spectrum [34]. A 22-dB gain is achieved and a NF of ~ 1.3 dB is realized in the experiment. Additionally, with the aim to cover a $P_{OA,in}$ range from -70 dBm to -35 dBm, we use two EDFAs (AEDFA-18, Amonics) for further amplification after the FOPA. VOA2 is used to tune the input optical power of EDFA2 for linear amplification and OBPF2 with a bandwidth of ~ 0.1 nm ultimately reduces the ASE noise. Then the analog optical signal propagates through a polarizer which filters the ASE noise orthogonal to the signal polarization state. Finally adjusted by VOA3, the amplified analog optical signal is fed into a PD (DET08CFC/M, Thorlab) with a fixed power of -5 dBm to minimize the nonlinearity. The RF spectrum of the AOL outputs is recorded by an electrical signal analyzer (N9030A, Keysight) with a minimum resolution of 1 Hz. All the fiber links are located on an anti-vibration optical table with air chambers to ultimately stabilize the system. Since the state of polarization of the optical field in each fiber drifts slightly after one hour, manual polarization alignment of the three waves is performed for the copier, FOPA and polarizer before each measurement of the AOL. For the practical transmission of optical signals with PS-FOPA, the pump can be attenuated by a designed in-line narrow-band notch filter to reduce the nonlinear optical effects in the fiber and then co-propagate with the signal and idler on a low-power level. At the Rx, the pump can be well regenerated using injection locking [35]. In this manner, the pump, signal and idler are still highly phase correlated. With proper dispersion compensation, this approach has been successfully demonstrated in long-haul optical communications [24].

In addition to the PS-FOPA, AOLs with PI-FOPA and EDFA are also implemented. To realize the PI-FOPA, the idler is filtered out by the OP and the PLL is turned off. The measured optical gain and NF of the PI-FOPA are ~ 16 dB and ~ 3.9 dB, respectively. For the EDFA-only-based AOL, the copier and FOPA stages are skipped and the output of the MZM is directly connected to VOA1. At the receiver side, the input optical signal is amplified by an EDFA (NF ~ 4.3 dB) and further amplified by another two EDFAs. The maximum gain of these tunable EDFAs is about 35 dB.

3.2. Experimental results

The output power of the RF signal and IMD3 as a function of RF input power for AOLs with different OPAs is shown by Fig. 6. The power of the Rx-input optical signal is -70 dBm, including both signal and idler for the PS-FOPA. The measured values are represented by squares and the solid lines are fitted curves. We estimated the noise floors by averaging the envelope of the RF noise spectrum around the central RF frequency with a span of 10 MHz. The blue, green and purple lines correspond to PS-FOPA, PI-FOPA and EDFA, respectively. As can be seen in Fig. (6), the PS-FOPA-based AOL exhibits ~ 4.9 dB and ~ 5.6 dB higher SNR than the AOLs with PI-FOPA and only EDFA, respectively. The link SFDR3 is 49.8 dB/Hz $^{2/3}$ when PS-FOPA is applied, while it drops to about 46.4 dB/Hz $^{2/3}$ for the case of PI-FOPA. It is further degraded to 45.9 dB/Hz $^{2/3}$ when only EDFAs are used. The back-to-back SFDR3 of the AOL without any optical amplification for the -5 dBm optical injection of the PD is about 100 dB/Hz $^{2/3}$. Although the link SFDR3 is greatly degraded by high link loss, the PS-FOPA can still improve the link performance to some extent over conventional EDFAs.

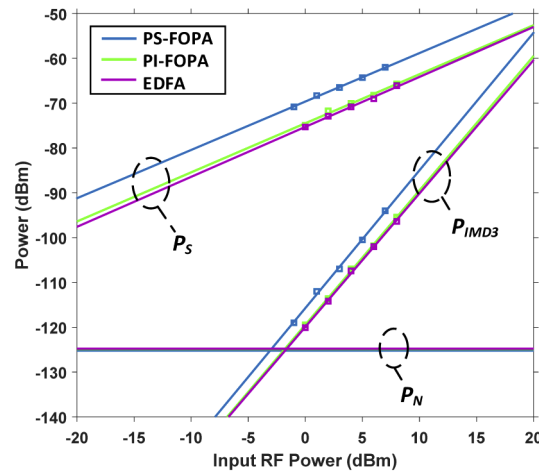


Fig. 6. Output power of the RF signal and IMD3 as a function of RF input power for AOLs with different OPAs. Square dots are measured values. Solid lines are fitted. The blue, green and purple lines correspond to cases of PS-FOPA, PI-FOPA and EDFA, respectively.

Figure 7(a) illustrates the SNR differences between the AOLs with various OPAs as a function of $P_{OA,in}$. The SNR curve of the PS-FOPA-based AOL acts as the baseline. The solid red and orange lines with squares are curves correspond to the PI-FOPA- and EDFA-based AOLs, respectively. With a -35-dBm Rx-input optical signal, the SNR difference is -2.9 dB for the case of EDFA. It drops gradually when $P_{OA,in}$ decreases from -35 dBm and reaches down to -5.5 dB at $P_{OA,in} = -70$ dBm. In other words, a 5.5-dB (4.9-dB) improvement in SNR is achieved using PS-FOPA instead of EDFA (PI-FOPA). In addition, the dotted red and orange lines are theoretical curves for the PI-FOPA- and EDFA-based AOLs, respectively. The measured SNR difference is in accordance with the theoretical prediction, although there are small gaps when the Rx-input optical signal power is less than -55 dBm. Besides, the SFDR3 differences between

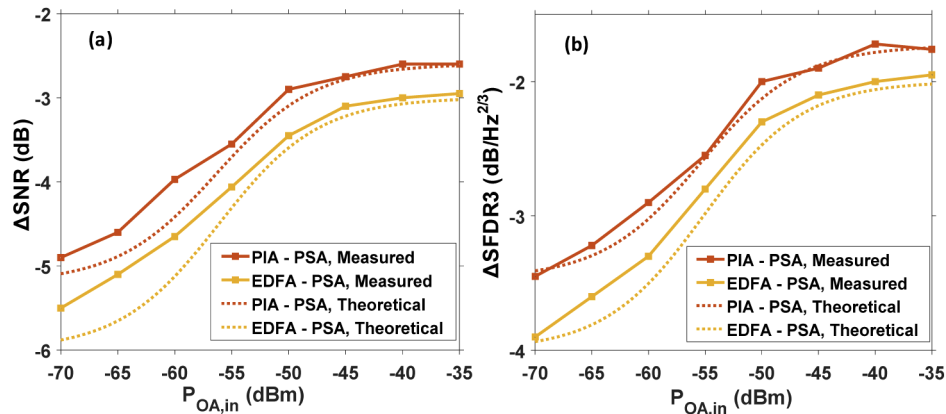


Fig. 7. (a) Measured Δ SNR and (b) Δ SFDR3 differences of the AOLs with various OPAs as a function of input Rx optical signal power. The SNR and SFDR3 of the PS-FOPA-based AOL is the baseline. The 3-dB optical bandwidth of the AOL is about 0.1 nm. The solid red and orange lines with squares are curves for PIA (PI-FOPA) versus PSA (PS-FOPA), and EDFA versus PSA, respectively. The dotted lines are theoretical curves.

the AOLs with PS-FOPA, PI-FOPA and EDFA are presented by Fig. 7(b). The SFDR3 of the PS-FOPA-based AOL is the baseline. As can be seen, the absolute value of the SFDR3 difference is $\sim 2 \text{ dB/Hz}^{2/3}$ for $P_{OA,in} = -35 \text{ dBm}$ and increases to $3.9 \text{ dB/Hz}^{2/3}$ when $P_{OA,in}$ drops to -70 dBm for the EDFA-based AOL. During the experiments, there is slight polarization drift between the signal and pump which induces fluctuations in the gain of FOPAs. Despite the gaps between the experimental and theoretical curves, which may be attributed to the polarization disturbance, noise estimation and non-ideal optical filtering, these measured results are still in general agreement with the theoretical expectations and shows that PS-FOPA has a potential to enhance the performance of AOLs with huge link losses.

4. Summary

A low-noise PS-FOPA-based AOL is investigated theoretically and demonstrated experimentally in this paper. The NF of PS-FOPA can break the 3-dB NF limit of conventional optical amplifiers and theoretically approach 0 dB. This can be utilized to improve the performance of the AOL in principle. Based on theoretical modeling, we find that the improvement in the SNR of AOL output signal can be $\sim 3 \text{ dB}$ with a 3-dB reduction of the OPA NF and can be enhanced to $\sim 6 \text{ dB}$ when the input optical signal power is in the weak regime where noise-noise beating dominates. Besides, the calculated SFDR3 of the AOL can be increased by 4 dB in this case. Furthermore, the improved performance of the AOL is realized in experiments with a 1.3-dB-NF PS-FOPA which has no pump dithering. The experimental results are in accordance with the theoretical analysis, which indicates that noiseless PS-FOPAs are promising in analog optical signal processing and microwave photonic systems.

Funding

Vetenskapsrådet (VR-2015-00535).

Acknowledgements

The authors thank Dr. Corentin Naveau, Kovendhan Vijayan, Zonglong He, Israel Rebolledo Salgado and Oskar Bjarki Helgasson for their help on experiments and discussions.

Disclosures

The authors declare no conflicts of interest.

References

1. J. Yao, "Microwave Photonics," *J. Lightwave Technol.* **27**(3), 314–335 (2009).
2. J. Capmany, G. Li, C. Lim, and J. Yao, "Microwave Photonics: Current challenges towards widespread application," *Opt. Express* **21**(19), 22862–22867 (2013).
3. D. Marpaung, J. Yao, and J. Capmany, "Integrated microwave photonics," *Nat. Photonics* **13**(2), 80–90 (2019).
4. Z. Tang, Y. Li, J. Yao, and S. Pan, "Photonics-Based Microwave Frequency Mixing: Methodology and Applications," *Laser Photonics Rev.* **14**(1), 1800350 (2020).
5. C. H. Cox, *Analog Optical Links: Theory and Practice* (Cambridge University, 2004).
6. A. Wiberg, "Generation, Modulation, and Detection of Signals in Microwave Photonic Systems," Chalmers University of Technology (PhD Thesis) (2008).
7. E. Xu, X. Zhang, L. Zhou, Y. Zhang, Y. Yu, X. Li, and D. Huang, "Ultrahigh-Q microwave photonic filter with Vernier effect and wavelength conversion in a cascaded pair of active loops," *Opt. Lett.* **35**(8), 1242–1244 (2010).
8. J. Dong, L. Liu, D. Gao, Y. Yu, A. Zheng, T. Yang, and X. Zhang, "Compact notch microwave photonic filters using on-chip integrated microring resonators," *IEEE Photonics J.* (2013).
9. A. M. Haimovich, R. S. Blum, and L. J. Cimini, "MIMO Radar with Widely Separated Antennas," *IEEE Signal Process. Mag.* **25**(1), 116–129 (2008).
10. P. Yin, X. Yang, Q. Liu, and T. Long, "Wideband distributed coherent aperture radar," in *IEEE Radar Conference*, 1114–1117 (2014).
11. F. Zhang, B. Gao, and S. Pan, "Photonics-based MIMO radar with high-resolution and fast detection capability," *Opt. Express* **26**(13), 17529–17540 (2018).

12. A. Wang, J. Wo, X. Luo, Y. Wang, W. Cong, P. Du, J. Zhang, B. Zhao, J. Zhang, Y. Zhu, J. Lan, and L. Yu, "Ka-band microwave photonic ultra-wideband imaging radar for capturing quantitative target information," *Opt. Express* **26**(16), 20708–20717 (2018).
13. C. Lim, M. Attygalle, A. Nirmalathas, D. Novak, and R. Waterhouse, "Analysis of optical carrier-to-sideband ratio for improving transmission performance in fiber-radio links," *IEEE Trans. Microwave Theory Tech.* **54**(5), 2181–2187 (2006).
14. H. V. Roussel, M. D. Regan, J. L. Prince, C. H. Cox, J. X. Chen, W. K. Burns, G. E. Betts, E. I. Ackerman, and J. C. Campbell, "Gain, Noise Figure and Bandwidth-Limited Dynamic Range of a Low-Biased External Modulation Link," in *IEEE International Topical Meeting on Microwave Photonics* (2007), pp. 84–87.
15. A. Karim and J. Devenport, "Noise Figure Reduction in Externally Modulated Analog Fiber-Optic Links," *IEEE Photonics Technol. Lett.* **19**(5), 312–314 (2007).
16. L. Xu, S. Jin, and Y. Li, "Down-conversion IM-DD RF photonic link utilizing MQW MZ modulator," *Opt. Express* **24**(8), 8405 (2016).
17. D. A. Tulchinsky, J. B. Boos, D. Park, P. G. Goetz, W. S. Rabinovich, and K. J. Williams, "High-Current Photodetectors as Efficient, Linear, and High-Power RF Output Stages," *J. Lightwave Technol.* **26**(4), 408–416 (2008).
18. M. Burla, C. Hoessbacher, W. Heni, C. Haffner, Y. Fedoryshyn, D. Werner, T. Watanabe, H. Massler, D. L. Elder, L. R. Dalton, and J. Leuthold, "500 GHz plasmonic Mach-Zehnder modulator enabling sub-THz microwave photonics," *APL Photonics* **4**(5), 056106 (2019).
19. V. J. Urick, M. E. Godinez, P. S. Devgan, J. D. McKinney, and F. Bucholtz, "Analysis of an Analog Fiber-Optic Link Employing a Low-Biased Mach-Zehnder Modulator Followed by an Erbium-Doped Fiber Amplifier," *J. Lightwave Technol.* **27**(12), 2013–2019 (2009).
20. G. P. Agrawal, *Fiber-Optic Communication Systems*, second, Wiley Online Books (1997).
21. C. J. McKinstrie, M. Yu, M. G. Raymer, and S. Radic, "Quantum noise properties of parametric processes," *Opt. Express* **13**(13), 4986–5012 (2005).
22. T. Umeki, H. Takara, Y. Miyamoto, and M. Asobe, "3-dB signal-ASE beat noise reduction of coherent multi-carrier signal utilizing phase sensitive amplification," *Opt. Express* **20**(22), 24727–24734 (2012).
23. Z. Tong, C. Lundström, P. A. Andrekson, C. J. McKinstrie, M. Karlsson, D. J. Blessing, E. Tipsuwannakul, B. J. Puttnam, H. Toda, and L. Grüner-Nielsen, "Towards ultrasensitive optical links enabled by low-noise phase-sensitive amplifiers," *Nat. Photonics* **5**(7), 430–436 (2011).
24. S. L. I. Olsson, H. Eliasson, E. Astra, M. Karlsson, and P. A. Andrekson, "Long-haul optical transmission link using low-noise phase-sensitive amplifiers," *Nat. Commun.* **9**(1), 2513 (2018).
25. B. Foo, M. Karlsson, K. Vijayan, M. Mazur, and P. A. Andrekson, "Analysis of nonlinearity mitigation using phase-sensitive optical parametric amplifiers," *Opt. Express* **27**(22), 31926–31941 (2019).
26. R. Kakarla, J. Schröder, and P. A. Andrekson, "Record-sensitivity Gb/s receiver for free-space applications based on phase-sensitive amplification," in *Conference on Lasers and Electro-Optics, OSA Technical Digest* (Optical Society of America, 2019), p. JTh5B.1.
27. O. Lim, V. Grigoryan, M. Shin, and P. Kumar, "Ultra-Low-Noise Inline Fiber-Optic Phase-Sensitive Amplifier for Analog Optical Signals," in *Conference on Optical Fiber Communication/National Fiber Optic Engineers Conference*, OSA Technical Digest (Optical Society of America, 2008), p. OML3.
28. A. Agarwal, T. Banwell, and T. K. Woodward, "RF Photonic Link Employing Optical Phase Sensitive Amplification," in *Optical Fiber Communication Conference, OSA Technical Digest* (Optical Society of America, 2012), p. OM3B.5.
29. L. Tarek, F. Ihsan, S. De, F. Goldfarb, and F. Bretenaker, "Optical Phase Sensitive Amplification for Microwave Photonics Applications: intermodulation distortion analysis," in *12th International Conference on Fiber Optics and Photonics, OSA Technical Digest* (Optical Society of America, 2014), p. S4A.3.
30. D. A. I. Marpaung, "High dynamic range analog photonic links: design and implementation," Twente University (PhD thesis) (2009).
31. <https://optical.communications.ii-vi.com/optical-instrumentation/waveshaper-4000a>.
32. J. Hansryd, P. A. Andrekson, M. Westlund, J. Li, and P.-O. Hedekvist, "Fiber-based optical parametric amplifiers and their applications," *IEEE J. Sel. Top. Quantum Electron.* **8**(3), 506–520 (2002).
33. C. Lundstrom, R. Malik, L. Gruner-Nielsen, B. Corcoran, S. L. I. Olsson, M. Karlsson, and P. A. Andrekson, "Fiber Optic Parametric Amplifier With 10-dB Net Gain Without Pump Dithering," *IEEE Photonics Technol. Lett.* **25**(3), 234–237 (2013).
34. D. M. Baney, P. Gallion, and R. S. Tucker, "Theory and Measurement Techniques for the Noise Figure of Optical Amplifiers," *Opt. Fiber Technol.* **6**(2), 122–154 (2000).
35. R. Kakarla, J. Schröder, and P. A. Andrekson, "Optical injection locking at sub nano-watt powers," *Opt. Lett.* **43**(23), 5769–5772 (2018).